Journal of Materials Chemistry

Cite this: DOI: 10.1039/c0jm04557h

www.rsc.org/materials

PAPER

WO_3 nanowires on carbon papers: electronic transport, improved ultraviolet-light photodetectors and excellent field emitters†

Liang Li,*[a] Yong Zhang,[b] Xiaosheng Fang,[a] Tianyou Zhai,[a] Meiyong Liao,[c] Xueliang Sun,*[b] Yasuo Koide,[c] Yoshio Bando[a] and Dmitri Golberg*[a]

Received 28th December 2010, Accepted 8th February 2011
DOI: 10.1039/c0jm04557h

Single-crystalline WO_3 nanowires were synthesized on carbon papers through a chemical vapor deposition process without using any catalysts. WO_3 nanowire field-effect transistors (FETs) were constructed to discuss the mechanism of electronic transport based on a thermal-activation model and a displacive transition. Photoconductive measurements showed that individual WO_3 nanowire photodetector was sensitive to the ultraviolet light, and the photoresponse was further improved using WO_3 nanowires on carbon papers, demonstrating significantly shortened response and decay times, and enhanced stability. Field-emission measurements showed that WO_3 nanowires were excellent field-emitters: an ultralow turn-on field of 1.8 V μm^{-1} and a threshold field of 3.3 V μm^{-1}, and a high field-enhancement factor of 6.9×10^3. These results indicate that present unique WO_3 nanowires on carbon papers are promising candidates for constructing high-performance electronic and optoelectronic devices.

Introduction

In the family of transition metal oxides, tungsten trioxides (WO_3) have attracted wide attention and substantial efforts have been devoted to fabricate one-dimensional (1D) WO_3 nanostructures for field emission, gas sensing, electrochromism, and photocatalysis.[1] The outstanding properties make WO_3 nanowires valuable as functional building blocks for the fabrication of optoelectronic nanodevices. Therefore, the investigation of electronic transport mechanisms of individual WO_3 nanowires is very important.[2] To accurately measure transport behaviors of WO_3 nanowires, it is essential to form ohmic contacts between nanowires and electrodes. However, this has achieved little success except for a recent work utilizing N-doped WO_3 nanowires to increase carrier concentration.[2]

1D oxide semiconductor nanomaterials are promising for field-emission applications due to their large aspect ratio, low work function, high mechanical stabilities, and high electrical and thermal conductivities.[3] The field-emission properties of 1D WO_3 nanostructures have been investigated recently, as shown in Table 2.[2,4] However, to meet demands of practical applications it is necessary to explore novel WO_3 nanostructures for further decreasing turn-on and threshold fields, increasing emission current density, and enhancing field-enhancement factor.

According to the range of wavelength, UV light is classified into UV-A (320–400 nm), UV-B (290–320 nm), and UV-C (200–290 nm), among which the UV-A light can easily reach the Earth's surface and may cause a skin cancer. Different from the visible light, people's eyes are blind to the UV-A light. Thus, the development of effective UV-A photodetectors (light sensors) is of great importance. With a wide bandgap $E_g \approx 3.3$ eV, WO_3 is applicable for detecting UV-A light. Up to now, there has been only a single literature with respect to the individual nanostructured WO_3 photodetector,[5] which showed the relatively slow response time of ~1 min. Thus, it is interesting to develop novel routes to optimize the performance of WO_3 photodetectors.

Herein, we fabricated the individual WO_3 nanowire field-effect transistors (FETs), from which the electrical transport mechanism was investigated based on temperature-dependent resistances. The individual WO_3 nanowire photodetectors showed sensing capability to UV-A light. Furthermore, we report a photoconductive nanodevice structure made of WO_3 nanowires on carbon papers, which demonstrated largely improved stability and shortened response time. Such novel hierarchical nanostructures were then used as excellent field-emitters: an ultralow turn-on field of 1.8 V μm^{-1} and threshold field of 3.3 V μm^{-1}, and a high field-enhancement factor of 6.9×10^3 were documented. These are the best field-emission parameters in all reported 1D WO_3 nanostructures. Our results demonstrate the

[a]*International Center for Materials Nanoarchitectonics (MANA), National Institute for Materials Science (NIMS), Namiki 1-1, Tsukuba, Ibaraki, 305-0044, Japan. E-mail: LI.Liang@nims.go.jp; Golberg.Dmitri@nims.go.jp*
[b]*Department of Mechanical and Materials Engineering, University of Western Ontario, London, Ontario, N6A 5B9, Canada. E-mail: xsun@eng.uwo.ca*
[c]*Sensor Materials Center, NIMS, Namiki 1-1, Tsukuba, Ibaraki, 305-0044, Japan*
† Electronic supplementary information (ESI) available. See DOI: 10.1039/c0jm04557h

uniqueness and effectiveness of WO_3 nanowires on carbon papers for optoelectronic applications.

Experimental

Material preparation and characterization

Uniform and aligned hierarchical WO_3 nanowires on carbon papers were synthesized by an improved chemical vapor deposition process without using catalysts.[6] The carbon paper coated with tungsten film was placed in the middle part of a quartz tube that was mounted horizontally inside a furnace. A carrier gas of high-purity Ar was passed through the quartz tube at a rate of 300 sccm (standard cubic centimetres per minute) for half an hour to purge the oxygen. After that, water vapor was introduced into the chamber with Ar and the system was heated to 750 °C for 1 h to induce the growth of tungsten oxide nanowires. After it was cooled to room temperature in the flowing carrier gas, the samples were annealed in air at 500 °C for 1 h to obtain WO_3 nanowires. The as-prepared WO_3 nanowires were analyzed by X-ray diffraction (XRD, Ultima IV/PSK), field-emission scanning electron microscopy (FE-SEM, Hitachi S-4800), and high-resolution transmission electron microscopy (HRTEM, JEM-3000F).

Device fabrication and properties

For field-effect transistor (FET) device fabrication, WO_3 nanowires were suspended in ethanol and then deposited on an oxidized Si substrate with a 200 nm thick SiO_2 layer that serves as a gate oxide. The standard photolithography technique followed by metal evaporation and lift-off procedures were used to define the source and drain electrodes and to electrically contact WO_3 nanowires. The *I–V* characteristics were recorded by room and low temperature (Nagase Electronic Equipments service, co.) probing systems and a semiconductor parameter analyzer (Keithley Instruments Inc).

For individual WO_3 nanowire photodetector fabrication, the FET device without gate voltage was illuminated with a light of different wavelengths at ambient atmosphere, and the photocurrent was recorded using a picoammeter R8340A and a dc voltage source R6144. A spectral response was recorded using a 500 W Ushio Xenon lamp with an illumination band width of 2 nm, and a monochromator with order sorting filters used. The light intensity was modulated through an aperture and calibrated by using a UV-enhanced Si photodiode.

Field-emission measurements were performed in a vacuum chamber at a pressure of 3×10^{-6} Pa. The WO_3 nanowires on carbon papers were directly attached to a cathode, and a Cu prober with a cross-section of 1 mm^2 was used as an anode. A dc voltage sweeping from 100 to 1100 V was applied to the samples, and a corresponding electronic current was recorded automatically.

Results and discussion

Fig. 1 shows the morphology, microstructure, and elemental maps of as-fabricated WO_3 nanowires. A low-magnification scanning electron microscopy (SEM) image reveals highly uniform and aligned hierarchical nanowires on carbon fibers (Fig. 1a). High-density WO_3 nanowires are covered on the whole carbon paper (the inset in Fig. 1a). Higher-magnification SEM image shows that dense and quasi-aligned nanowires intersect each carbon fiber throughout (Fig. 1b). An X-ray diffraction (XRD) pattern indicates that WO_3 nanowires have a monoclinic phase (JCPDS card No. 89-4476) (Fig. 1c). A high-resolution transmission electron microscopy (HRTEM) image and a selected-area electron diffraction (SAED) pattern (Fig. 1d and insets) indicate that nanowires are single crystals with the preferred [002] growth direction. Fig. 1e and 1f show the elemental maps of individual nanowires, indicating uniform distribution of the constituting W and O elements.

Fig. 2a represents a typical SEM image of an individual WO_3 nanowire FET device. The WO_3 nanowire was connected by Cr/Au electrodes patterned on a SiO_2/Si substrate using a standard photolithography process. The current–voltage (*I–V*) curves under different gate voltages (V_g) are shown in Fig. 2b. The linear curves indicate the good Ohmic contacts between the WO_3 nanowire and the electrodes. It can be seen that the conductance of nanowires increases monotonically as the gate voltage increases, indicating an n-type character of the as-fabricated nanowires. The transfer characteristic of FET is weak (not shown here). Electrical transport mechanism was investigated by the temperature-dependent resistance (*R-T*) measured on the FET device without applying gate voltages. Fig. S1 (ESI†) shows the *I–V* characteristics of WO_3 nanowires in the temperature range of 10–296 K. The linear *I–V* curves show that the characteristics fit the Ohm's law, from which the resistivity of the nanowire can be calculated as $\rho = (R \times S)/L$ (ρ: resistivity, *R*: resistance, *S*: cross-sectional area, *L*: length of the nanowire). Assuming that the WO_3 nanowires are of circular cross section, the calculated resistivity is ~18.2 Ω cm at room temperature. Fig. S2 shows the *I–V* characteristics measured from eight devices labeled from S0 to S7 in Fig. S3. Clearly all the devices comply with Ohm's law. The diameters of the nanowires vary from 95 nm to 140 nm. The calculated resistivities of the nanodevices are listed in Table 1. The resistivity values are between 18.2 Ω cm and 70.6 Ω cm.

Based on *I–V* results, the *R–T* curve (Fig. 2c) was plotted. It demonstrates the typical semiconductor character except for a phase transition near 45 K. In general, the electronic transport of transition-metal oxides is governed by the hopping conduction mechanism and the electrons are the major carriers *via* the oxygen vacancies. The thermal-activation model predicts that the conductivity follows the equation[7]

$$\sigma = \sigma_0 \exp\left(\frac{-\Delta E}{kT}\right) \quad (1)$$

where σ is the conductivity, *k* is the Boltzmann constant, and ΔE is the activation energy. The linear curve ($\ln(1/R) \approx 1000/T$) in Fig. 2d suggests that the transport mechanism is dominated by thermal activation at relatively high temperatures (45–296 K). From the slope of this curve, the activation energy of $\Delta E \sim 0.06$ eV is estimated. The extremely low activation energy implies good conduction capability of an individual WO_3 nanowire. Near 45 K, resistance anomaly is observed, possibly arising from a displacive transition that also occurs in the bulk WO_3 single crystals.[8] Phase transitions in tungsten trioxide are often associated with distortions of the oxygen octahedral that surround

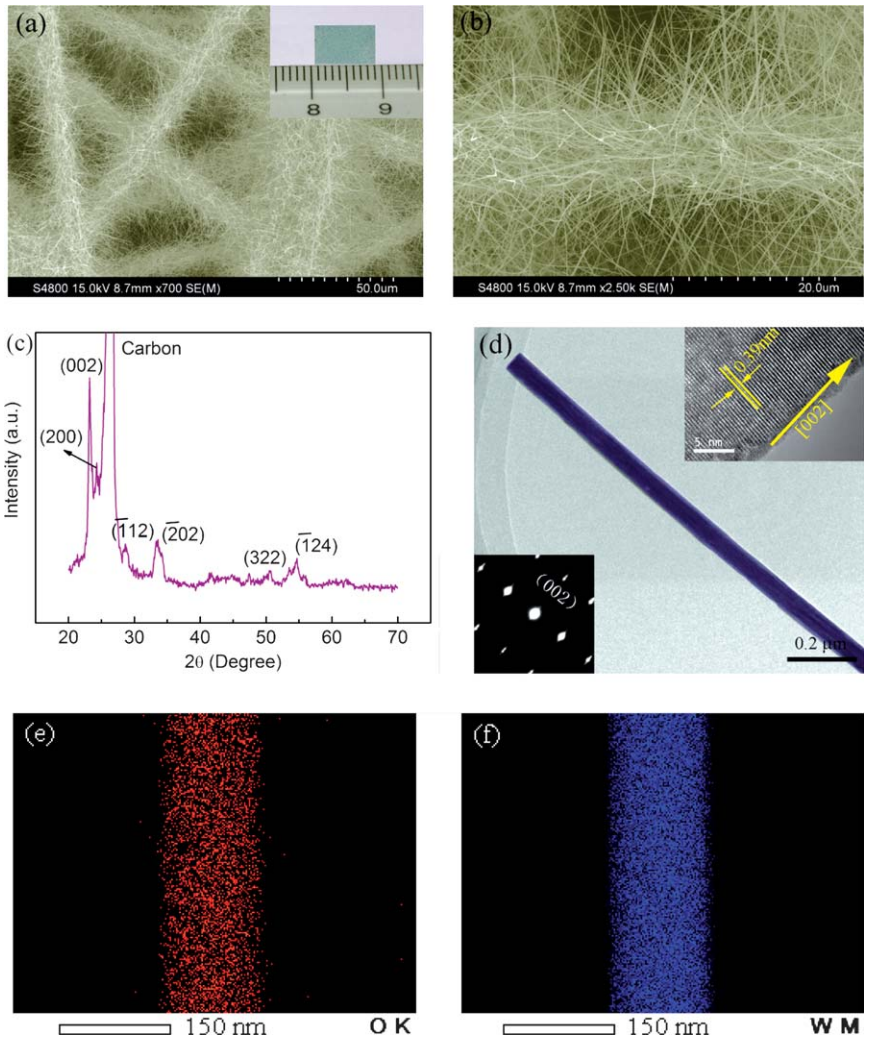

Fig. 1 (a) Low- and (b) high- magnification SEM images of as-prepared nanowires, and (c) corresponding XRD pattern. (d) HRTEM image and SAED pattern of an individual WO_3 nanowire. e) O and W elemental maps.

the heavy W atoms, and with changes in unit cell multiplicity.[8,9] In a low-temperature region ($T < 25$ K), $\ln(1/R)$ is independent of temperature, which indicates that the number of thermal-activation carriers is too low to affect the total amount of carriers.

Fig. 3a shows a schematic measurement configuration of an individual WO_3 nanowire photodetector. A monochromatic light was introduced to vertically illuminate the nanowire and the corresponding I–V curves were recorded. Fig. 3b shows the responsivity of the WO_3 nanowire measured at 1.0 V. With decreasing wavelength, the sensitivity increases gradually and reaches the maximum value at ~375 nm (3.3 eV, close to bandgap of WO_3) and then drops, implying a band-gap excitation related process. The decreased sensitivity at a wavelength shorter than 375 nm is attributed to the enhanced absorption of high energy photons near the surface region of the semiconductor.[10] Fig. 3c shows the I–V curves of the photodetector illuminated with a light of various wavelengths and under dark condition. A photo-excited current is higher than the dark current. All these results indicate that the present photodetector demonstrates a selectivity and sensitivity towards the UV-A light. To examine the reproducibility of individual WO_3 nanowire photodetectors, we randomly measured the photoresponse of devices S3 and S4 (Fig. S4, ESI†). It can be clearly seen that these curves have the similar varying trend with decreasing wavelength of light from 380 nm to 250 nm, implying the same bandgap-excited sensing mechanism.

Photoresponse depends on the light intensity. Fig. 3d represents I–V curves of the nanowire illuminated by a 375 nm light with various intensities from 0.08 to 1.65 mW cm^{-2}. The corresponding dependence of a photocurrent on light intensity can be fitted to a power law (Fig. 3e), $I_p \sim P^{\theta}$, where θ determines the response of the photocurrent to light intensity. The fitting gives a nearly linear behavior with $\theta = 1.0$.

The photoresponse switching behavior of the WO_3 nanowire photodetector is shown in Fig. 3f, which illustrates that the photocurrent can be reproducibly switched "ON" and "OFF" by periodically modulating the 375 nm light at a low bias voltage of 10.0 V. From this response curve, it is difficult to estimate response and decay times (t_r and t_d) (the time for the current increasing from 10% to 90% of the peak value or *vice versa* is defined as the t_r and t_d, respectively), because we cannot observe stable platforms of the photocurrent and the dark current during a period of measurements. In general, under the dark condition,

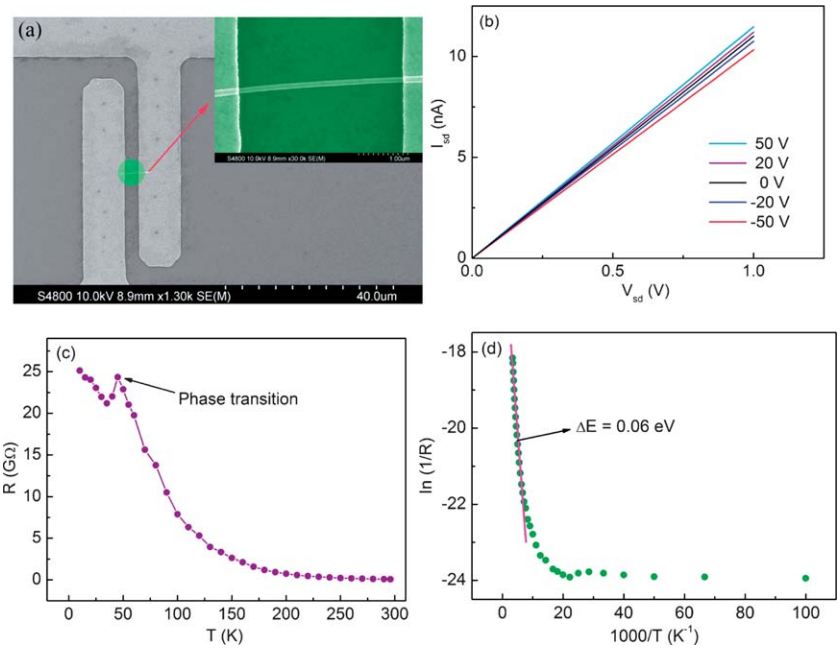

Fig. 2 (a) Typical SEM image of a FET device. The top-right inset is an enlarged view. (b) *I–V* plots under different gate voltages. (c) A curve of *R versus T*. (d) ln(1/*R*) as a function of 1000/*T*.

Table 1 Calculated resistivities of eight nanodevices labeled from S0 to S7

Nanodevices	Resistance/MΩ	Resistivity/Ω cm
S0	76.5	18.2
S1	117.4	46.5
S2	181.4	39.9
S3	156.1	70.6
S4	240.5	35.9
S5	145.5	35.8
S6	111.0	34.5
S7	105.9	34.7

a low conductance is caused by the depletion layer formed near the surface by adsorbed oxygen molecules in the n-type semiconductor [$O_2(g) + e^- \rightarrow O_2^-(ad)$]. Upon light illumination with photon energy higher than the bandgap, adsorbed oxygen ions discharge by photo-generated holes [$h^+ + O_2^- \rightarrow O_2(g)$], enhancing the conductance.[11]

Fig. 3g shows the schematic of a photodetector constructed directly using WO_3 nanowires on carbon papers. The metal electrode on the top surface was fabricated by a mask-assisted electron beam deposition, and the uncovered area was illuminated by 375 nm light to induce photocurrent. Between the carbon paper and the top-surface electrode, the nanowire lengths are enough to join neighboring nanowires and form many nanowire/nanowire junctions. These junctions act as electrical conducting paths for electrons. This design is very simple and efficient compared with an individual nanostructure device. In other words, individual nanostructure devices are usually fabricated either by tedious and time-consuming photo or electron-beam lithography processes including a series of steps such as synthesis, dispersal of nanostructures, spin coating of photo resist, exposure, and so on.[12] More importantly, such device demonstrated a significantly improved photoresponse compared with the individual WO_3 nanowire photodetector. Fig. 3h illustrates a time-dependent photocurrent of this device measured at 10.0 V under a 375 nm-light "ON" and "OFF". The response and decay times are about 3 s and 20 s, respectively. In comparison with individual WO_3 nanowire photodetectors (Fig. 3f), the response and decay time, stability, and reproducibility are largely enhanced.

Field-emission measurements show that WO_3 nanowires on carbon papers are excellent field-emitters. Fig. 4a shows the field-emission current density *J versus* the applied field *E* at an anode-cathode distance of 250 μm. The current density gradually increases with increasing voltage, and a turn-on field at a current density of 10 μA cm^{-2} and a threshold field at a current density of 1 mA cm^{-2} are as low as 1.8 V μm^{-1} and 3.3 V μm^{-1}, respectively. To reveal the field-emission mechanism, the corresponding curve $\ln(J/E^2) - (1/E)$ is plotted (the inset in Fig. 4a) based on the Fowler–Nordheim (*FN*) theory:[13]

$$J = (A\beta^2E^2/\phi)\exp(-B\phi^{3/2}/\beta E) \quad (2)$$

Here $A = 1.54 \times 10^{-6}$ A eV V^{-2}, $B = 6.83 \times 10^3$ $eV^{-3/2}$ V μm^{-1}, ϕ is the work function of the emitting materials (5.7 eV), and β is the field-enhancement factor that is related to the emitter geometry, crystal structure, and spatial distribution of the emitting centers. Here β is as high as 6.9×10^3. The linear variation of $\ln(J/E^2)$ with $1/E$ (*FN* plot) confirms that the emission-current is due to the electron tunneling effect. Stability of the field-emitters is another important parameter related to potential applications. Field-emission stability measurement of WO_3 nanowires was performed by keeping a current density at 8.0 mA cm^{-2} over 12 h. As shown in Fig. 4b, there is no large current degradation or notable fluctuation during this period. The good emission stability promises that present WO_3 nanowires are good candidates in the cold-cathode-based panel display devices.

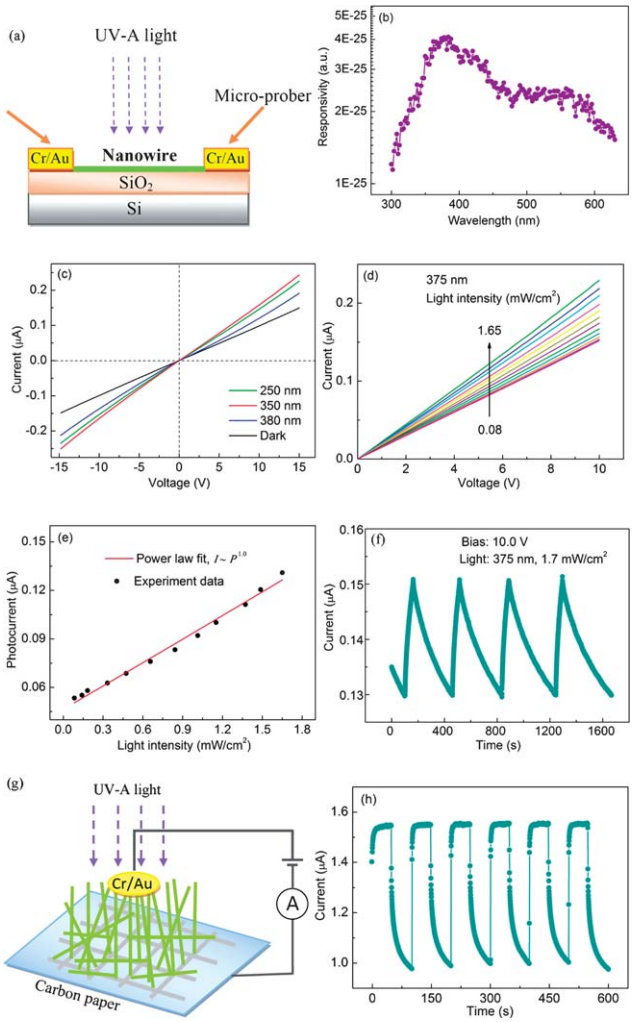

Fig. 3 (a) Schematic of measuring photoconductivity on an individual WO_3 nanowire. (b) Spectral response of the device, demonstrating a band-gap excited process. (c) *I–V* curves of the individual WO_3 nanowire photodetector under dark condition and light with various wavelengths. (d) *I–V* curves of a WO_3 nanowire photodetector under 375 nm light irradiation of various intensities. (e) Photocurrent as a function of light intensity and corresponding fitting curve using the power law. (f) Time response of a WO_3 nanowire photodetector. (g) Schematic of photodetector constructed directly using WO_3 nanowires on carbon papers, and (h) corresponding light switching "ON" and "OFF" curve.

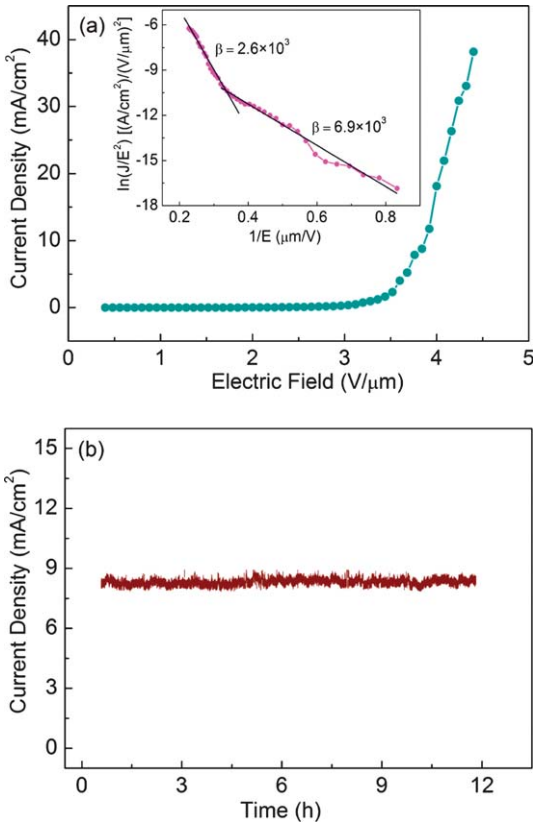

Fig. 4 (a) A *J–E* curve of WO_3 nanowires. The inset is a $\ln(J/E^2) - (1/E)$ plot from Fowler–Nordheim equation. (b) A stable current emission over 12 h.

These field-emission parameters are the best among 1D WO_3 nanostructures (Table 2), and even surpass those of other reported semiconductors such as ZnO, Si, carbon nanotubes, and so on.[14] Such excellent performances are mainly attributed to a large aspect-ratio, quasi-aligned arrays, and direct contact between WO_3 nanowires and conductive carbon papers.

Conclusions

In summary, individual WO_3 nanowire FET was constructed to investigate the type and mechanism of conductance, which was discussed in the frame of a thermal-activation model and

Table 2 Comparison of the field-emission parameters between this work and previous studies of 1D WO_3 nanostructures. We define the turn-on and threshold field at a field producing an emission current density of 10 μA cm^{-2} and 1 mA cm^{-2}, respectively. If the other values are used, it is marked

ID WO_3 nanostructures	Turn-on field/V μm^{-1}	Threshold field/V μm^{-1}	Field-enchancement factor (β)	Reference
Nanowires & nanorods	2	—	5.0×10^3	4
	13	—	6.7×10^2	4
	4.1	—	2.1×10^3	4
	3.6	—	2.7×10^3	4
	4.8	—	—	4
	—	4.5	—	4
	—	4.3 at 10 mA cm^{-2}	1.7×10^3	2
	6.44	9.42 at 10 mA cm^{-2}	7.0×10^2	2
	1.8	3.3	6.9×10^3	Present work

a displacive transition. Individual WO_3 nanowire photodetector showed high potential for sensing UV-A light. Photoconductive characteristics, including a spectra response, *I–V* curves under different light intensities, and time response were studied. Improved photodetectors were fabricated directly using WO_3 nanowires on carbon papers, demonstrating significantly enhanced stability and shortened response and decay times. Field-emission measurements showed that such hierarchical WO_3 nanostructures have an ultralow turn-on field of 1.8 V μm^{-1} and a threshold field of 3.3 V μm^{-1}, and a high field-enhancement factor of 6.9×10^3. These results demonstrate that WO_3 nanowires on carbon papers are promising candidates for constructing novel electronic and optoelectronic nanoscale devices.

Acknowledgements

This work was supported by the International Center for Materials Nanoarchitectonics (MANA) of the National Institute for Materials Science (NIMS), Tsukuba, Japan. X. S. Fang thanks the JSPS financial support (No. 22760517). X. L. Sun thanks NSERC Canada Research Chair program.

References

1 J. Polleux, A. Gurlo, N. Barsan, U. Weimar, M. Antonietti and M. Niederberger, *Angew. Chem., Int. Ed.*, 2006, **45**, 261; J. Zhou, Y. Ding, S. Z. Deng, L. Gong, N. S. Xu and Z. L. Wang, *Adv. Mater.*, 2005, **17**, 2107; Z. G. Zhao and M. Miyauchi, *Angew. Chem., Int. Ed.*, 2008, **47**, 7051.

2 M. T. Chang, L. J. Chou, Y. L. Chueh, Y. C. Lee, C. H. Hsieh, C. D. Chen, Y. W. Lan and L. J. Chen, *Small*, 2007, **3**, 658; S. J. Wang, W. J. Lu, G. Cheng, K. Cheng, X. H. Jiang and Z. L. Du, *Appl. Phys. Lett.*, 2009, **94**, 263106.

3 J. H. He, T. H. Wu, C. L. Hsin, K. M. Li, L. J. Chen, Y. L. Chueh, L. J. Chou and Z. L. Wang, *Small*, 2006, **2**, 116; Y. L. Chueh, L. J. Chou, S. L. Cheng, J. H. He, W. W. Wu and L. J. Chen, *Appl. Phys. Lett.*, 2005, **86**, 133112; J. C. She, Z. M. Xiao, Y. H. Yang, S. Z. Deng, J. Chen, G. W. Yang and N. S. Xu, *ACS Nano*, 2008, **2**, 2015; Y. H. Yang, B. Wang, N. S. Xu and G. W. Yang, *Appl. Phys. Lett.*, 2006, **89**, 043108.

4 D. Lu, A. Ogino, B. Liang, J. Liu and M. Nagatsu, *Jpn. J. Appl. Phys.*, 2009, **48**, 090206; D. Lu, B. Liang, A. Ogino and M. Nagatsu, *J. Vac. Sci. Technol., B: Microelectron. Nanometer Struct.–Process., Meas., Phenom.*, 2010, **28**, C2A98; Y. Kojima, K. Kasuya, T. Ooi, K. Nagato, K. Akayama and M. Nakao, *Jpn. J. Appl. Phys.*, 2007, **46**, 6250; K. Huang, Q. Pan, F. Yang, S. Ni and D. He, *Mater. Res. Bull.*, 2008, **43**, 919; K. Huang, Q. Pan, F. Yang, S. Ni and D. He, *Phys. E.*, 2007, **39**, 219; Y. H. Baek and K. J. Yong, *J. Phys. Chem. C*, 2007, **111**, 1213; J. Chen, Y. Y. Dai, J. Luo, Z. L. Li, S. Z. Deng, J. C. She and N. S. Xu, *Appl. Phys. Lett.*, 2007, **90**, 253105; X. Zhang, L. Gong, K. Liu, Y. Cao, X. Xiao, W. Sun, X. Hu, Y. Gao, J. Chen, J. Zhou and Z. L. Wang, *Adv. Mater.*, 2010, **22**, 5292.

5 K. Huang, Q. Zhang, F. Yang and D. Y. He, *Nano Res.*, 2010, **3**, 281.

6 Y. Zhang, Y. G. Chen, H. Liu, Y. Q. Zhou, R. Y. Li, M. Cai and X. L. Sun, *J. Phys. Chem. C*, 2009, **113**, 1746.

7 N. F. Mott, *J. Non-Cryst. Solids*, 1968, **1**, 1.

8 I. Lefkowitz, M. B. Dowell and M. A. Shields, *J. Solid State Chem.*, 1975, **15**, 24.

9 S. Sawada, *J. Phys. Soc. Jpn.*, 1956, **11**, 1237; S. Tanisaki, *J. Phys. Soc. Jpn.*, 1960, **15**, 566; S. Tanisaki, *J. Phys. Soc. Jpn.*, 1960, **15**, 573.

10 H. Kind, H. Q. Yan, B. Messer, M. Law and P. D. Yang, *Adv. Mater.*, 2002, **14**, 158; J. S. Jie, W. J. Zhang, Y. Jiang, X. M. Meng, Y. Q. Li and S. T. Lee, *Nano Lett.*, 2006, **6**, 1887.

11 C. Soci, A. Zhang, B. Xiang, S. A. Dayeh, D. P. R. Aplin, J. Park, X. Y. Bao, Y. H. Lo and D. L. Wang, *Nano Lett.*, 2007, **7**, 1003.

12 Y. Ye, L. Dai, T. Sun, L. P. You, R. Zhu, J. Y. Gao, R. M. Peng, D. P. Yu and G. G. Qin, *J. Appl. Phys.*, 2010, **108**, 044301; S. Liu, J. Ye, Y. Cao, Q. Shen, Z. Liu, L. Qi and X. Guo, *Small*, 2009, **5**, 2371; L. Li, P. C. Wu, X. S. Fang, T. Y. Zhai, L. Dai, M. Y. Liao, Y. Koide, H. Q. Wang, Y. Bando and D. Golberg, *Adv. Mater.*, 2010, **22**, 3161; T. Y. Wei, C. T. Huang, B. J. Hansen, Y. F. Lin, L. J. Chen, S. Y. Lu and Z. L. Wang, *Appl. Phys. Lett.*, 2010, **96**, 013508; A. Manekkathodi, M. Y. Lu, C. W. Wang and L. J. Chen, *Adv. Mater.*, 2010, **22**, 4059; L. Li, P. S. Lee, C. Y. Yan, T. Y. Zhai, X. S. Fang, M. Y. Liao, Y. Koide, Y. Bando and D. Golberg, *Adv. Mater.*, 2010, **22**, 5145.

13 J. P. Liu, X. T. Huang, Y. Y. Li, X. X. Ji, Z. K. Li, X. He and F. L. Sun, *J. Phys. Chem. C*, 2007, **111**, 4990; L. Li, T. Y. Zhai, H. B. Zeng, X. S. Fang, Y. Bando and D. Golberg, *J. Mater. Chem.*, 2011, **21**, 40; X. S. Fang, Y. Bando, U. K. Gautam, C. H. Ye and D. Golberg, *J. Mater. Chem.*, 2008, **18**, 509.

14 X. S. Fang, Y. Bando, C. H. Ye, G. Z. Shen, U. K. Gautam, C. C. Tang and D. Golberg, *Chem. Commun.*, 2007, 4093; Y. B. Tang, H. T. Cong and H. M. Cheng, *Appl. Phys. Lett.*, 2006, **89**, 093113; B. Xiang, Q. X. Wang, Z. Wang, X. Z. Zhang, L. Q. Liu, J. Xu and D. P. Yu, *Appl. Phys. Lett.*, 2005, **86**, 243103; B. Q. Zeng, G. Y. Xiong, S. Chen, W. Z. Wang, D. Z. Wang and Z. F. Ren, *Appl. Phys. Lett.*, 2006, **89**, 223119.

